Kinematics of gas and stars in the circumnuclear starforming ring of NGC 3351

(submitted to MNRAS)

Guillermo F. Hägele

Ángeles I. Díaz, Mónica V. Cardaci, Elena Terlevich and Roberto Terlevich

UAM - ESAC - INAOE

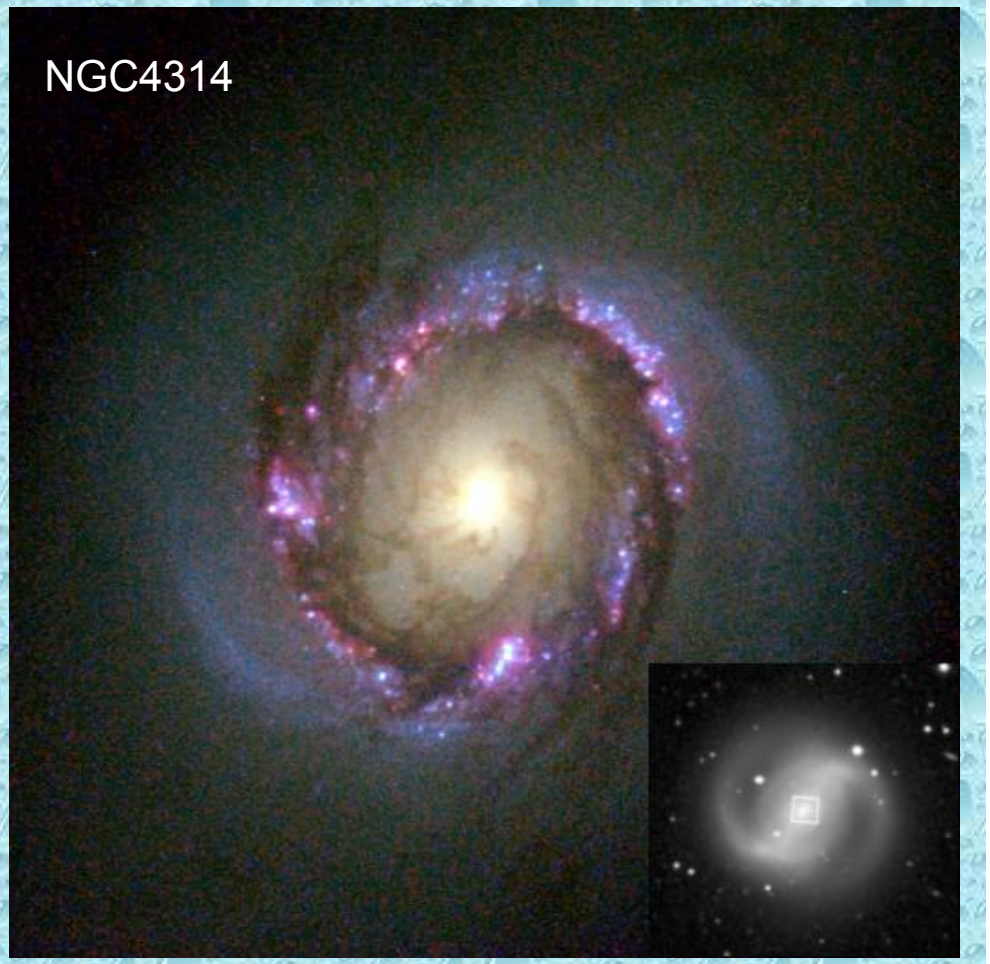
Introduction

The **bulges** of some nearby **spiral galaxies** show intense starforming regions located in a roughly **annular pattern** around their nuclei.

At **optical wavelengths**, these circumnuclear starforming regions (CNSFRs) **are** easily **observable rings**.

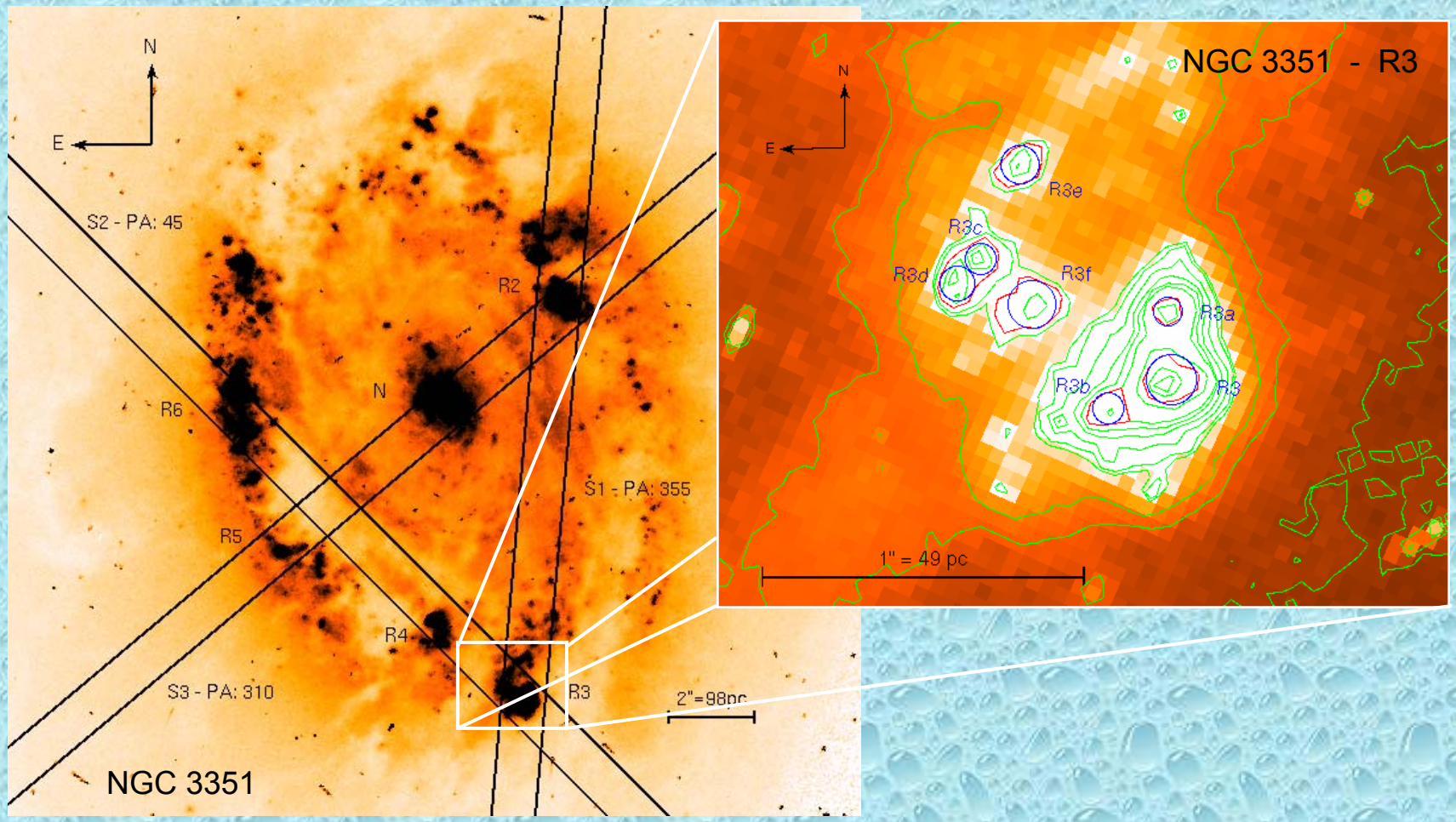
In the **UV**, **massive stars dominate the observed circumnuclear emission even in the presence of an active nucleus** (González-Delgado et al., 1998.ApJ.505.174; Colina et al., 2002ApJ.579.545).

Cid-Fernándes et al. (2001ApJ.558.81) for a representative sample of 35 **Seyfert 2 galaxies**, find that **about 40%** of them **show** unambiguous **evidence of circumnuclear star formation** within 300pc of the nucleus and that **these starforming regions contribute about 30 to 50% to the Hβ total emission** of the central zone.



Introduction

These **CNSFRs**, with **sizes going from a few tens to a few hundreds of pc** (e.g., Díaz & Pérez-Montero, 2000MNRAS.312.130) **seem to be made of several HII regions ionised by luminous compact stellar clusters** whose sizes, as measured from high spatial resolution HST images, are seen to be **of only a few pc**.

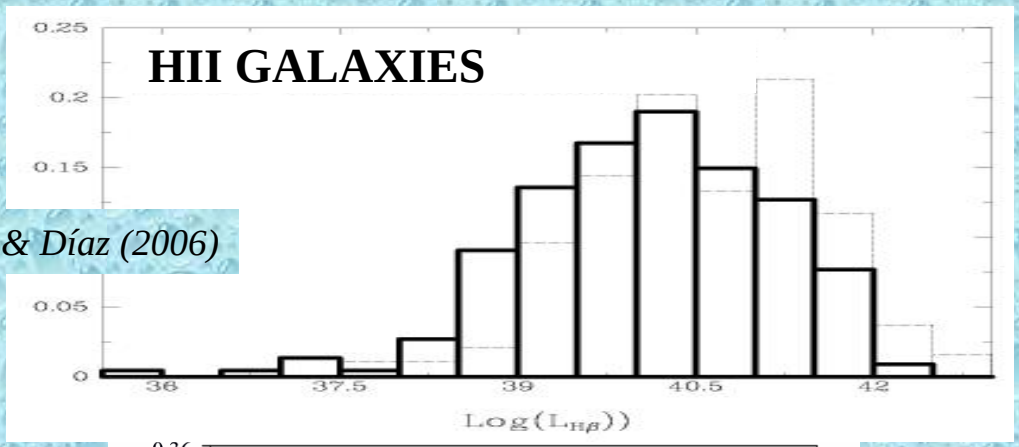


Introduction

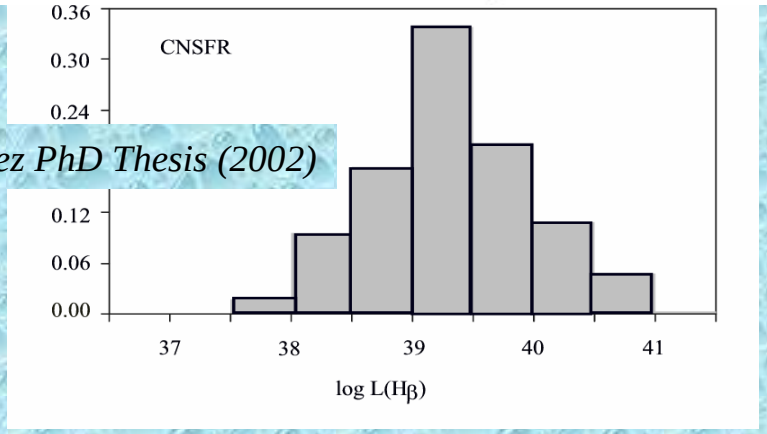
Their masses, as derived with the use of **population synthesis models** in circumnuclear regions of different galaxies, **suggest that these clusters are gravitationally bound** and that they might evolve into globular cluster configurations (Maoz et al., 1996AJ.111.2248).

The luminosities of CNSFRs are rather large with M_V between -12 and -17 and **Hβ luminosities** between **2×10^{38} and 7×10^{40}** erg s^{-1}.

These values are **comparable to** those shown by **30 Dor**, the largest HII region in the LMC, **and overlap** with those shown by **HII galaxies** (Melnick et al., 1988MNRAS.235.297, Díaz et al., 2000MNRAS.311.120, Hoyos & Díaz, 2006MNRAS.365..454, and references therein).



Hoyos & Díaz (2006)



Álvarez-Álvarez PhD Thesis (2002)

Introduction

Although these HII regions are very luminous not much is known about their kinematics or dynamics for both the ionised gas and the stars.

It could be said that **the worst known parameter** of these ionising clusters is **their mass**.

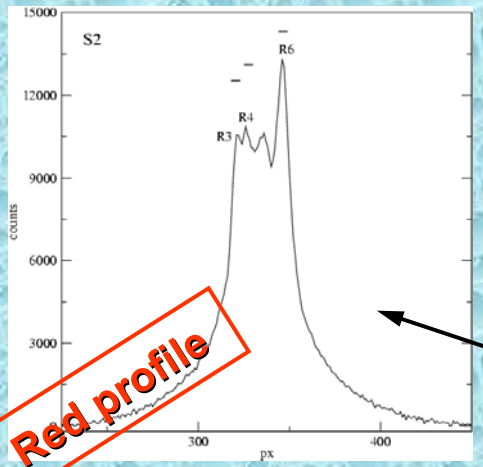
There are different methods to estimate the mass of a stellar cluster. **Classically one assumes that the system is virialized and determines the total mass inside a radius by applying the virial theorem to the observed velocity dispersion of the stars** (σ_*).

σ_* is hard to measure in young stellar clusters (a few Myr old) due to the shortage of prominent stellar absorption lines.

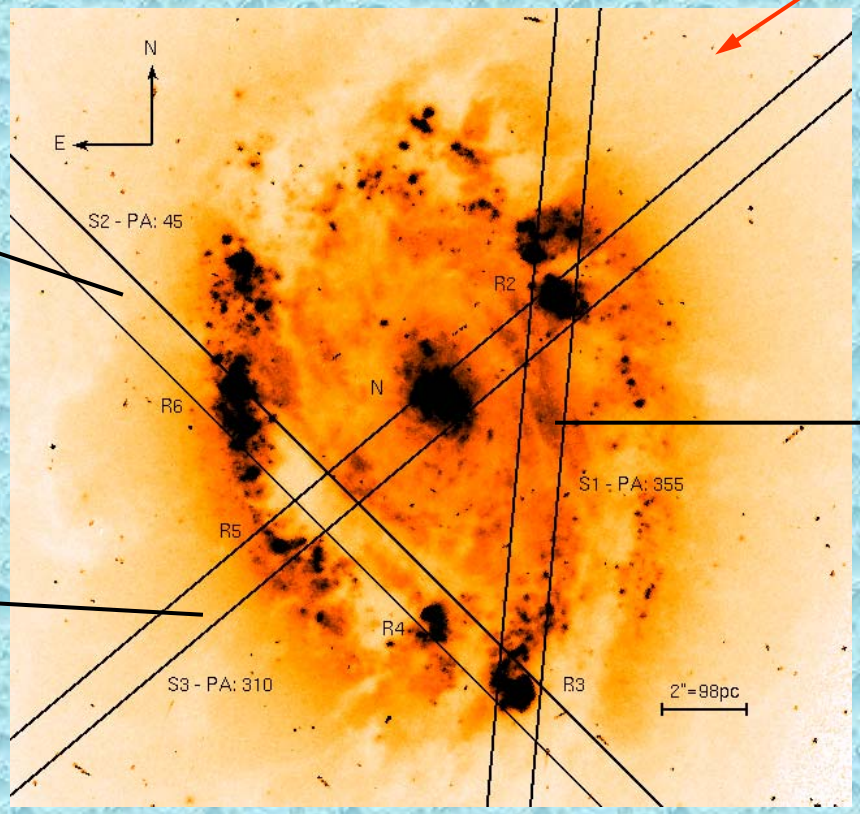
At IR wavelengths (~8500Å) the contamination due to nebular lines is much smaller and since red supergiant stars, if present, dominate the near-IR light where the **CaII λλ8498, 8542, 8662**Å triplet lines (CaT) are found, these should be easily observable allowing the determination of σ_* (Ho & Filippenko, 1996ApJ.466.83).

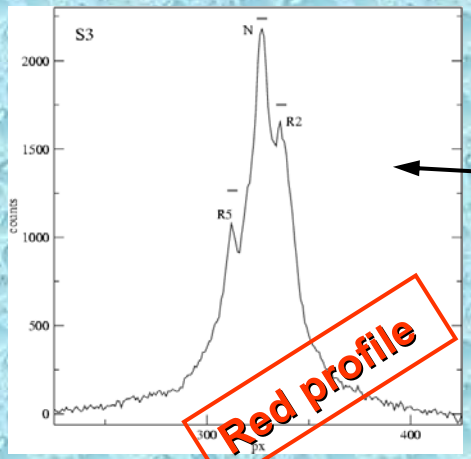
Observations

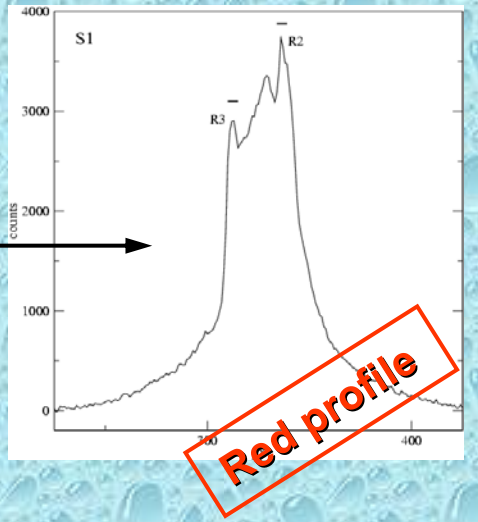
High resolution blue and far-red spectra (**0.2** and **0.36** Å/px) were acquired simultaneously using the blue and red arms of ISIS, mounted on the 4.2m William Herschel Telescope (WHT), for **five CNSFRs and the nucleous** of NGC 3351.



F606W – HST image

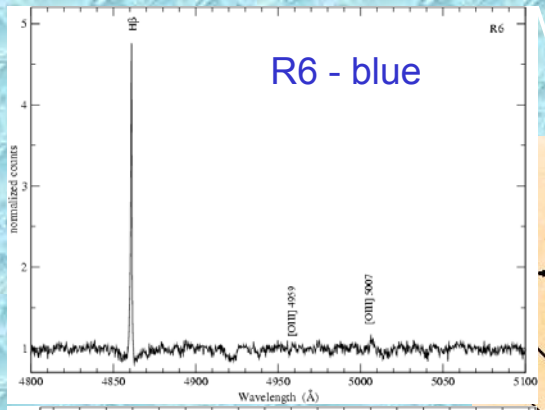


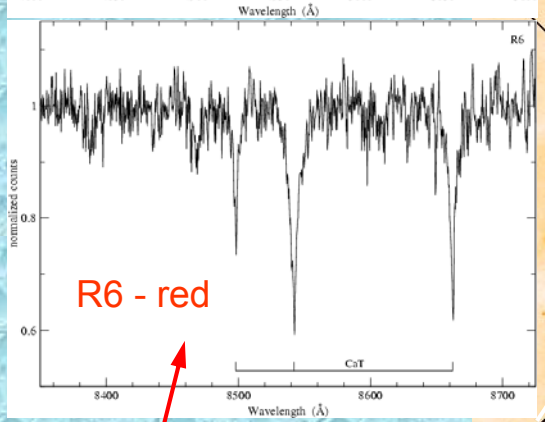




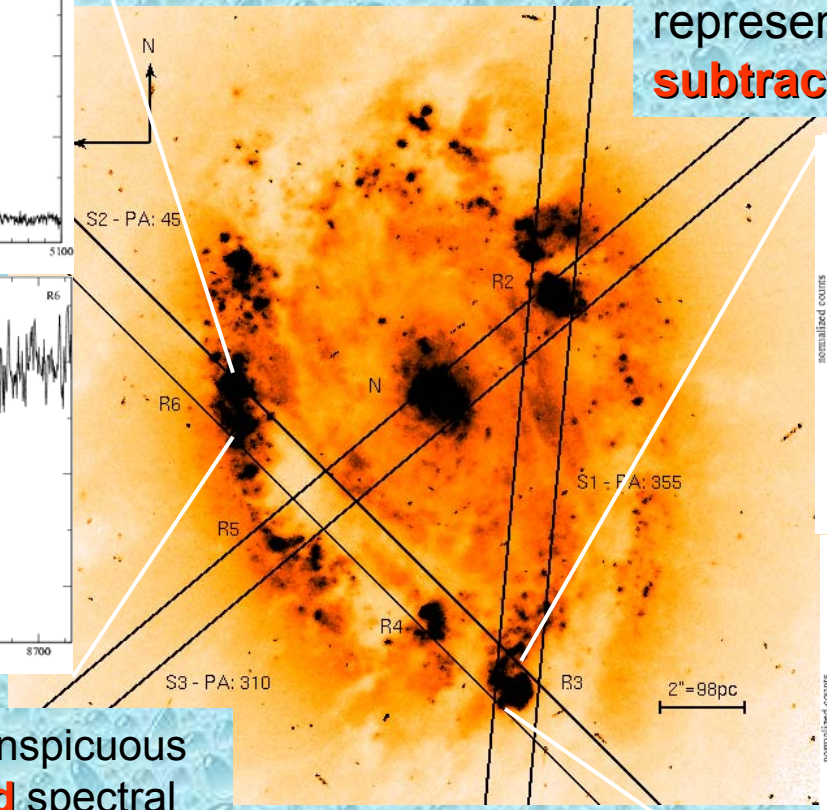
Observations

In some cases, the CaT lines are **contaminated by Paschen emission** which occur at wavelengths very close to those of the CaT lines.

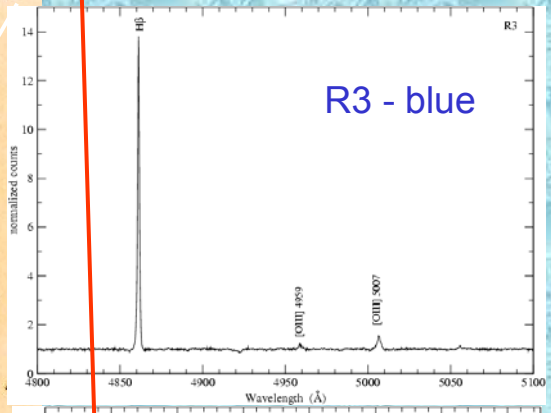


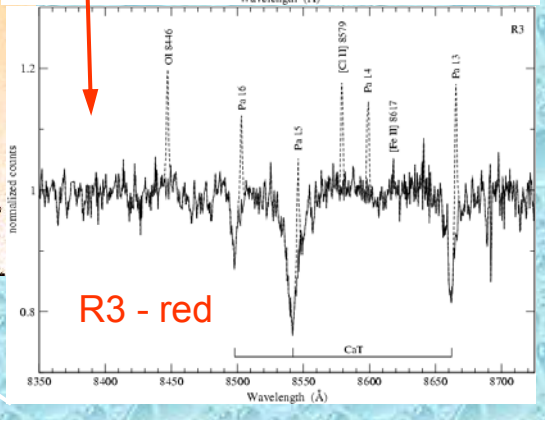


Notice the **absence** of conspicuous **emission lines in the red** spectral range for this region.



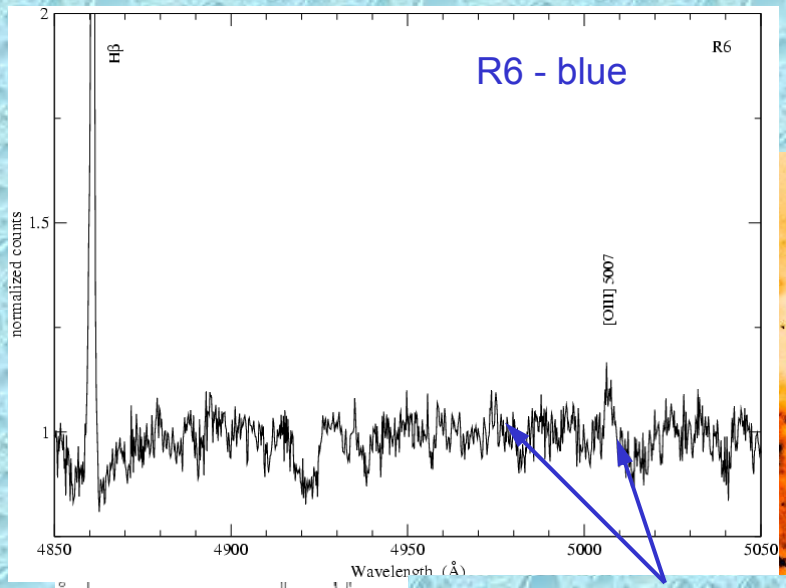
The dashed line shows the obtained spectrum; the solid line represents the **spectrum after subtracting the emission lines**.



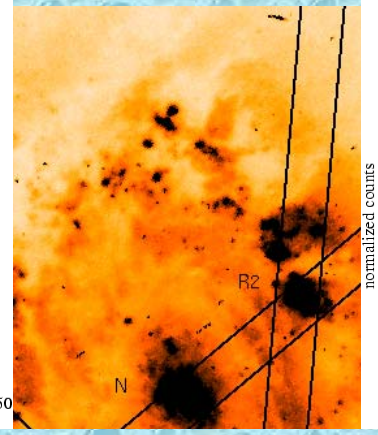


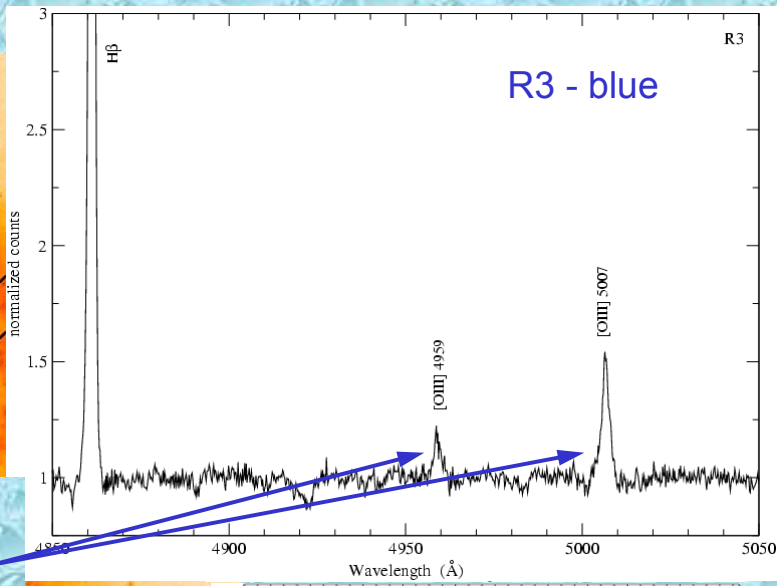
Observations

In some cases, the CaT lines are **contaminated by Paschen emission** which occur at wavelengths very close to those of the CaT lines.

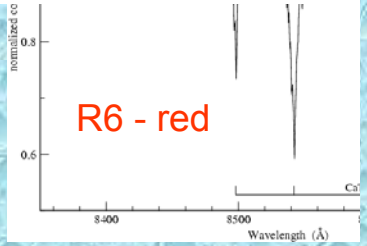


R6 - blue



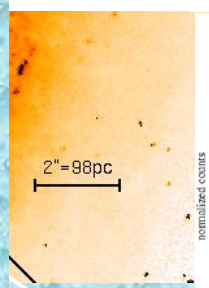


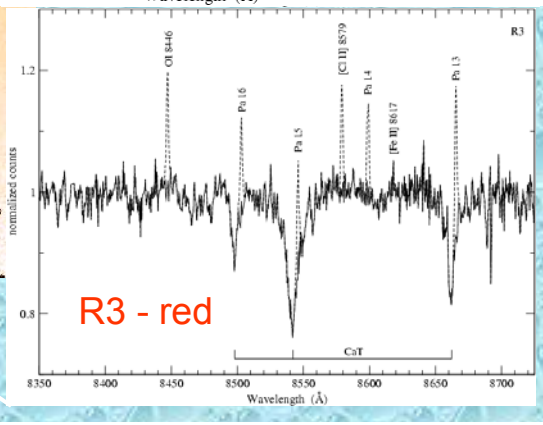
R3 - blue



R6 - red

Due to the **high metallicity** of the CNSFRs (Díaz et al., 2006astro-ph/0610787), the lines of oxygen are seen to be very weak and, in some cases, **only the strongest λ5007**Å is detected.

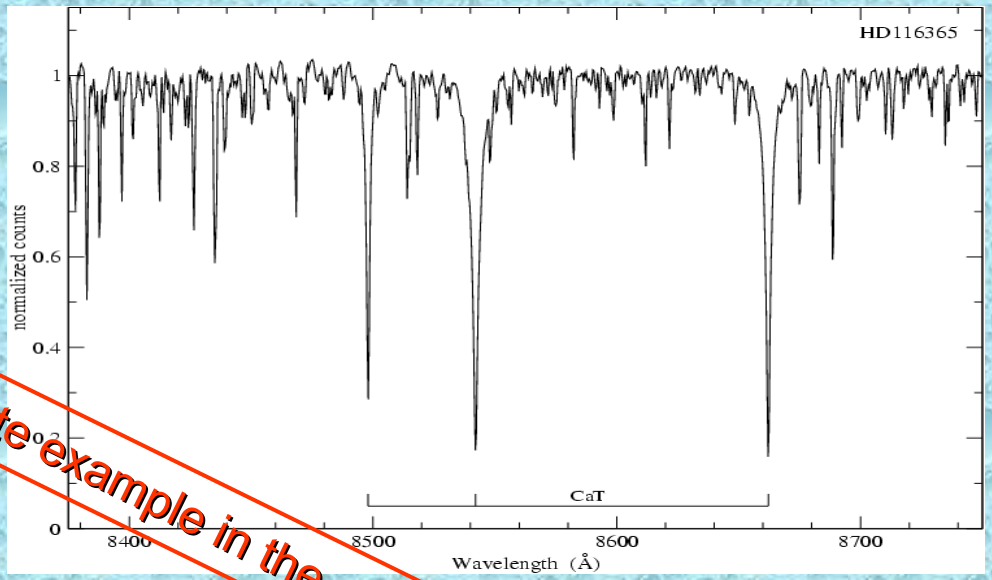




R3 - red

Observations

Observations of 11 template velocity stars were made (4 during the first night and 7 during the second) **to provide good stellar reference frames** in the same system as the galaxy spectra for the kinematic analysis in the far red. They are late type giant and supergiant stars which have strong CaT features (Díaz et al.,1989MNRAS.239.325).



Template example in the red range

Results: Kinematics of stars and ionised gas

Stellar radial velocities and velocity dispersions were obtained from the absorption CaT lines using the cross-correlation technique described in detail by Tonry & Davis (1979AJ.84.1511), **with** the **variations** introduced by Nelson & Whittle (1995.ApJSS.99.67) and Palacios et al. (1997.A&A.323.749).

The wavelength and the width of the Hβ and [OIII] λ5007Å emission lines were measured to determine both the radial velocities and velocity dispersions (σ_{gas}) of the ionised gas **fitted a Gaussian to the whole line**.

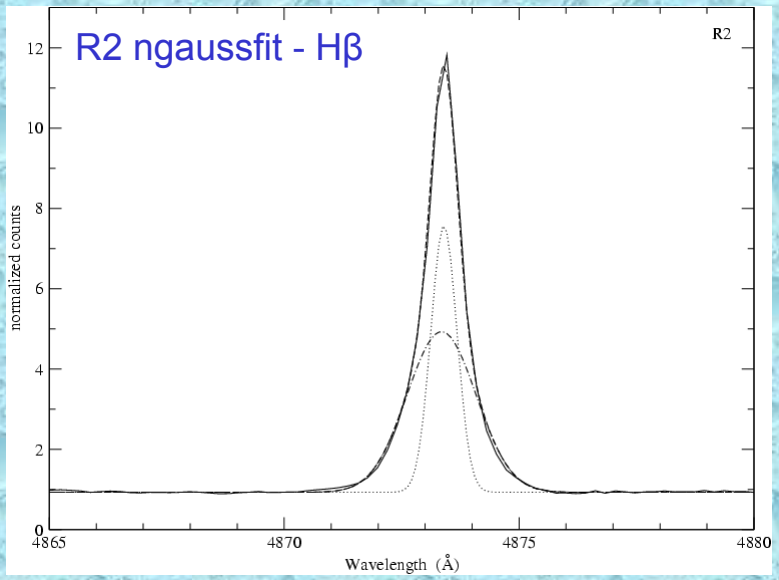
We determined the line of sight stellar and gas velocity along each slit. Extractions were made every two pixels for slit position S1. For slit positions S2 and S3 they were made every three pixels, with one pixel overlap between consecutive extractions. In this way the signal to noise ratio and the spatial resolution were optimised.

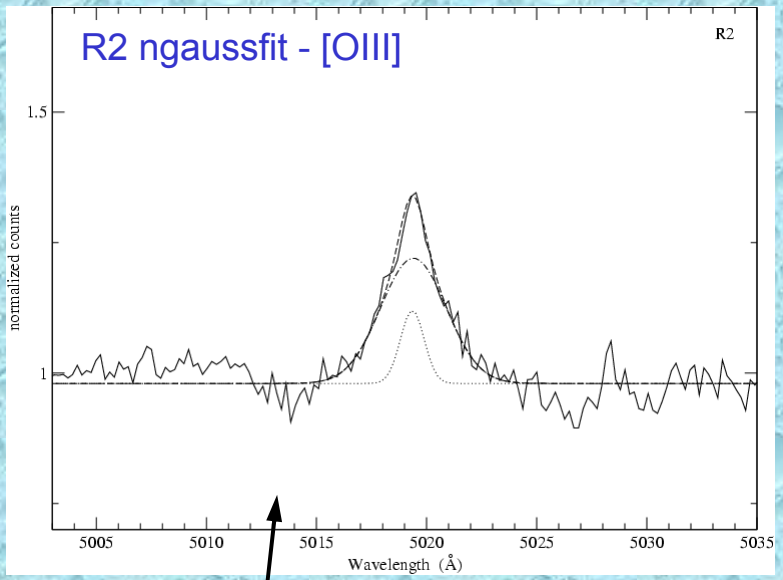
σ_* and σ_{gas} was estimated at the position of **each CNSFR** and the nucleus **using apertures of 5px**, which correspond to **1.0" x 1.8" and 1.0" x 1.9"**, respectively.

Results: ionised gas - ngaussfit

Unexpectedly, the Gaussian fit revealed the presence of **more than one component** in the **Hβ** lines. **The optimal fit was found for two different components for all the regions**.

We then **used the widths of those components to fit the [OIII]** lines finding also optimal fits for regions **R2 and R3**.



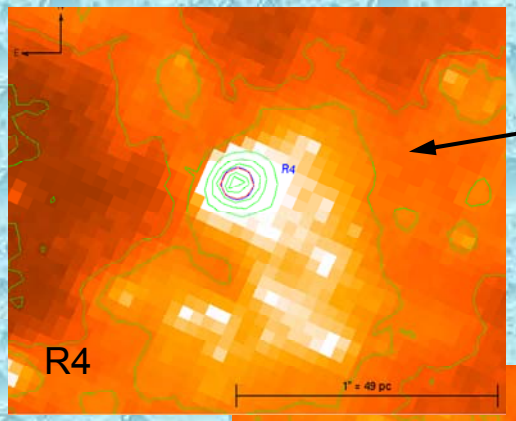


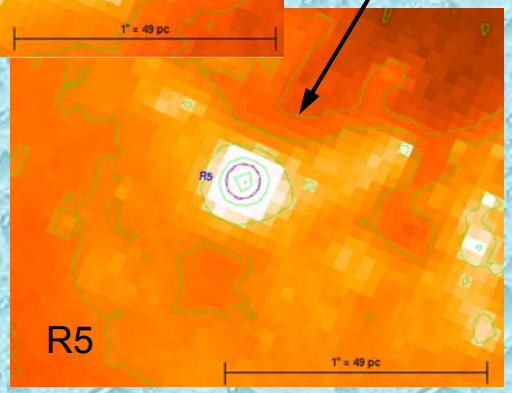
For the rest of the regions the two component fit did not show any improvemt over the single component one, probably due to the low signal-to-noise ratio.

Results: sizes

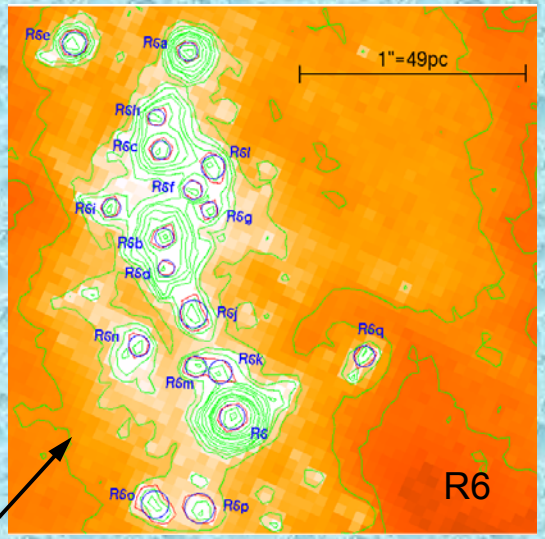
We have **defined** the radius (**R**) of a given structure as in Meurer et al. (1995AJ.110.2665) assuming that they have an intrinsically circularly symmetric Gaussian profile and **superposing the contours in the F606W WFPC2-HST image and determining the half light strength** between the peak of the intensity for each region and the galaxy background.

We find, as expected, that several of these regions are composed of more than one knot.





Only **R4** and **R5** seem to have a **unique principal knot**.

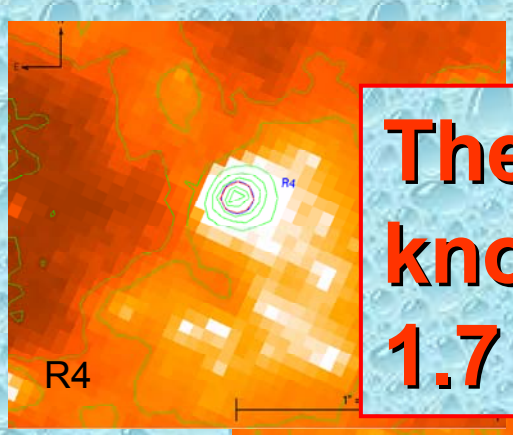


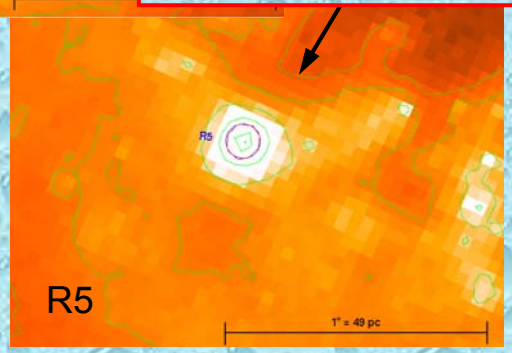
In the most **extreme case**, **R6**, we find **at least 18 knots**.

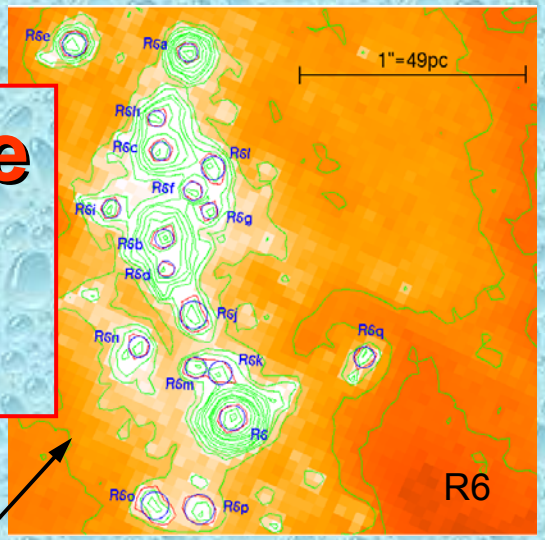
Results: sizes

We have **defined** the radius (**R**) of a given structure as in Meurer et al. (1995AJ.110.2665) assuming that they have an intrinsically circularly symmetric Gaussian profile and **superposing the contours in the F606W WFPC2-HST image and determining the half light strength** between the peak of the intensity for each region and the galaxy background.

We find, as expected, that **several of these regions are composed of more than one knot**.







The radii of the single knots vary between 1.7 and 4.9 pc.

In the most **extreme case**, **R6**, we find **at least 18 knots**.

Results: Masses

- **We have used the virial theorem to estimate upper limits to the dynamical masses** (M_*) inside the half light radius (R) for each observed knot in the HST image.

$$M_* = 3\,\sigma_*\,R / G \qquad \text{(Ho \& Filippenko, 1996ApJ.466L.83)}$$

In order to do this, we have assumed that the systems are spherically symmetric, gravitationally bound and have isotropic velocity distribution.

- **We have derived the masses of the ionising star clusters** (M_{ion}) **from the total number of ionising photons**.

$$M_{ion} = \frac{7.35\times10^{11}\,L(H\alpha)}{10^{44.8+0.86\log[EW(H\beta)]}}$$

from Leitherer et al. (1995ApJS.96.9) $Q(H_0)$

from Díaz (1998.Ap&SS.263.143) $Q(H_0)/M_{ion}$

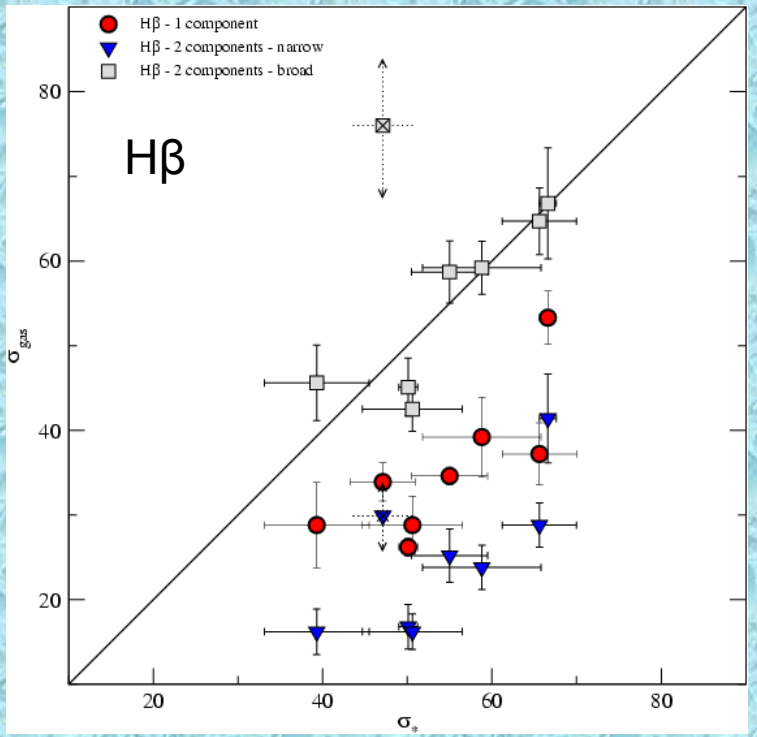
- **The amount of ionised gas** (M_{HII}) **associated to each starforming region complex has been obtained from Hα luminosities**.

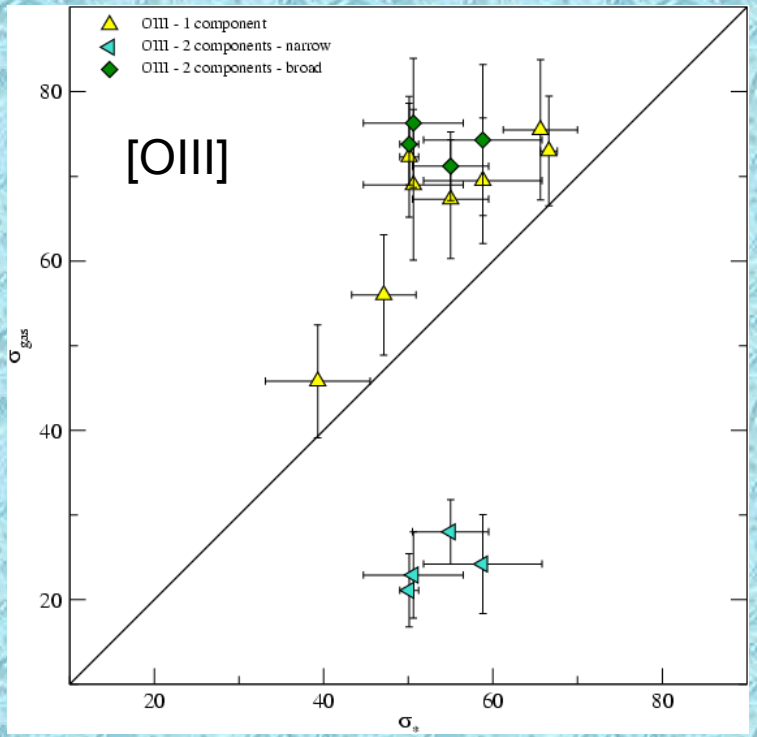
$$M_{HII} = 3.32\times10^{-33}\,L(H\alpha)\,N_e^{-1} \qquad \text{(Macchetto et al. 1990ApJ.356.389)}$$

L(Hα) from Planesas et al. (1997.A&A.325.81); EW(Hβ) from Pérez-Olea (1996. PhD Thesis); N_e from Díaz et al. (2006astro-ph/0610787).

Summary & Conclusions

Stellar velocity dispersions are between 39 and 67 km/s, **about 20 km/s larger than those measured for the gas**. However, **the best Gaussian fits involved two different components for the gas: a ``broad component'' with a velocity dispersion similar to that measured for the stars**, and **a ``narrow component'' with a dispersion lower than the stellar one by about 30 km/s**.

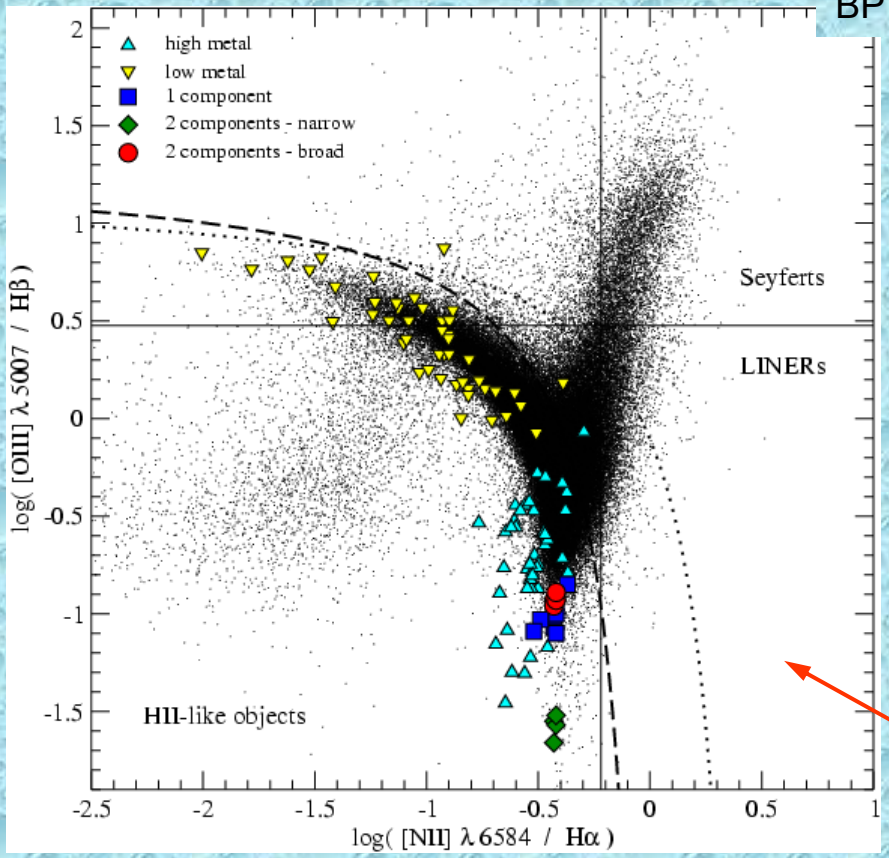




Summary & Conclusions

When plotted in a [OIII]/Hβ vs. [NII]/Hα diagram (BPT, Baldwin, Phillips & Terlevich, 1981PASP.93.5), **the two systems are clearly segregated with the narrow component having the lowest excitation and being among the lowest excitation line ratios detected within the SDSS dataset of starburst systems**.

BPT diagram

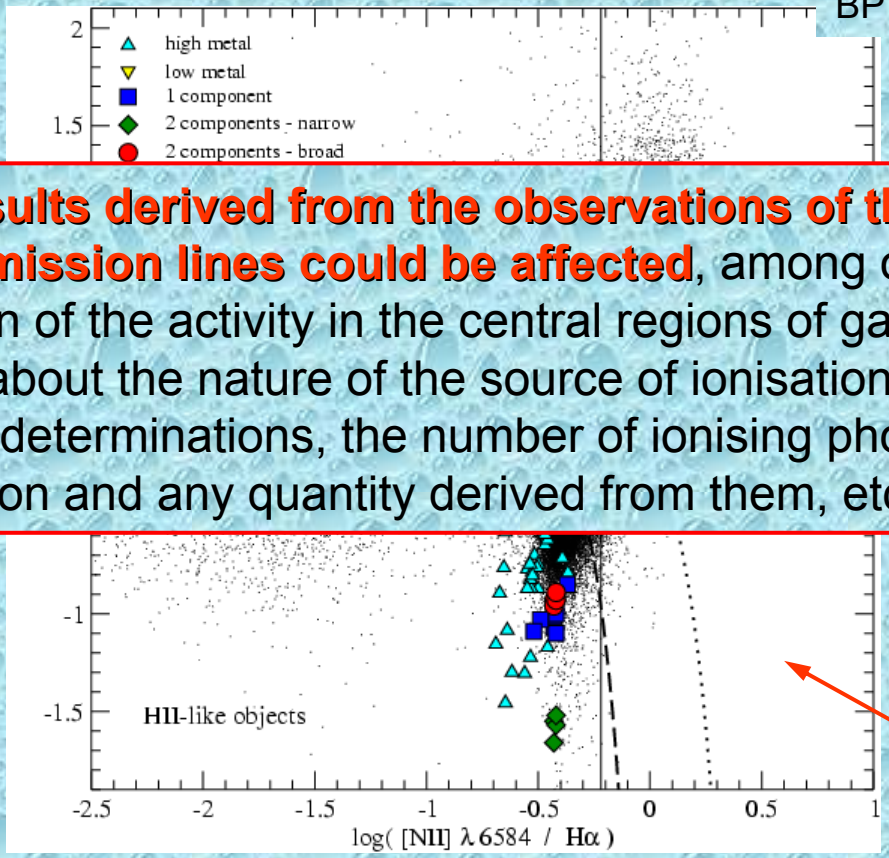


SDSS data from López (2005.MSc.Thesis.INAOE)

Summary & Conclusions

When plotted in a [OIII]/Hβ vs. [NII]/Hα diagram (BPT, Baldwin, Phillips & Terlevich, 1981PASP.93.5), **the two systems are clearly segregated with the narrow component having the lowest excitation and being among the lowest excitation line ratios detected within the SDSS dataset of starburst systems**.

BPT diagram



Several results derived from the observations of the different emission lines could be affected, among others: the classification of the activity in the central regions of galaxies, the inferences about the nature of the source of ionisation, the gas abundance determinations, the number of ionising photons from a given region and any quantity derived from them, etc.

SDSS data from López (2005.MSc.Thesis.INAOE)

Summary & Conclusions

Values for the **dynamical masses** are in the range **between 4.9×10^6 and 4.3×10^7 $M_\odot$** for the **CNSFRs** and is 3.5×10^7 $M_\odot$ for the nuclear region inside the inner 11.3pc. Masses derived **from the Hβ** velocity dispersion under the assumption of a **single component** for the gas **would have been underestimated by factors between approximately 2 to 4**.

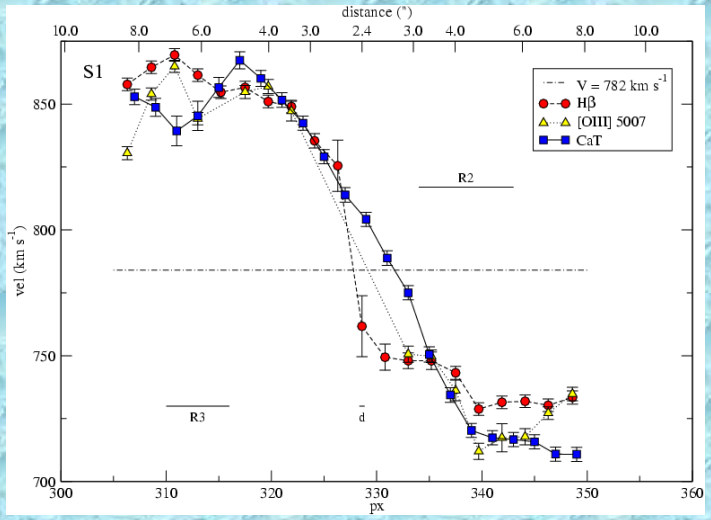
The derived masses for the individual clusters of NGC 3351 are **between 1.8 and 8.7×10^6 $M_\odot$. These values are between 5.5 and 26 times the mass derived for the SSC A in NGC 1569 by Ho & Filippenko** (1996ApJ.466L.83) and larger than other kinematically derived SSC masses.

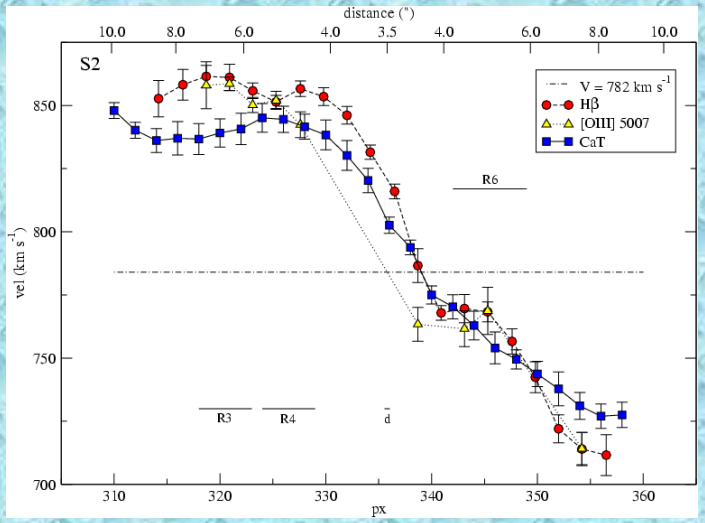
Masses of the ionising stellar clusters are between 4.1×10^5 and 2.4×10^6 $M_\odot$ for the starforming regions, and is 3.1×10^5 $M_\odot$ for the nucleus, **comparable to that derived by González-Delgado et al.** (1994.ApJ.437.239) for the circumnuclear region A in NGC 7714.
Therefore, the ratio of the ionising stellar population to the total dynamical mass is between 0.01 and 0.11.

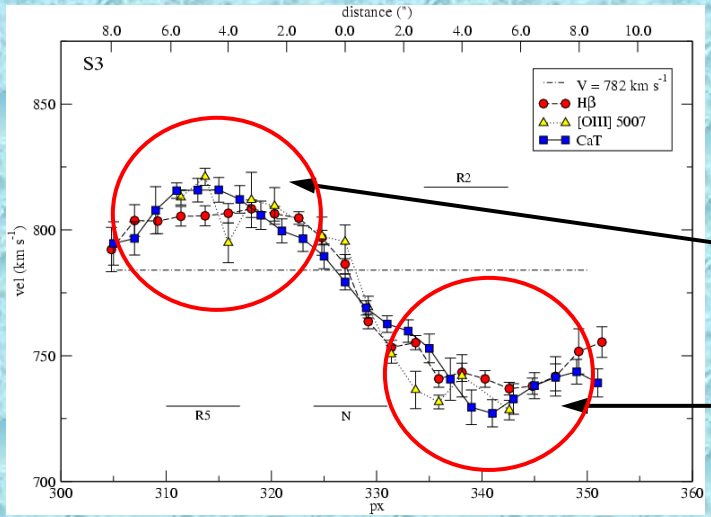
Derived masses for the ionised gas vary between 3×10^3 and 8.6×10^4 $M_\odot$ for the CNSFRs, and is 1×10^3 $M_\odot$ for the nucleus, **also comparable to that derived by González-Delgado et al.** (1994.ApJ.437.239).

Summary & Conclusions

The rotation velocities derived for both stars and gas are in reasonable agreement, although in some cases the gas shows a velocity slightly different from that of the stars.



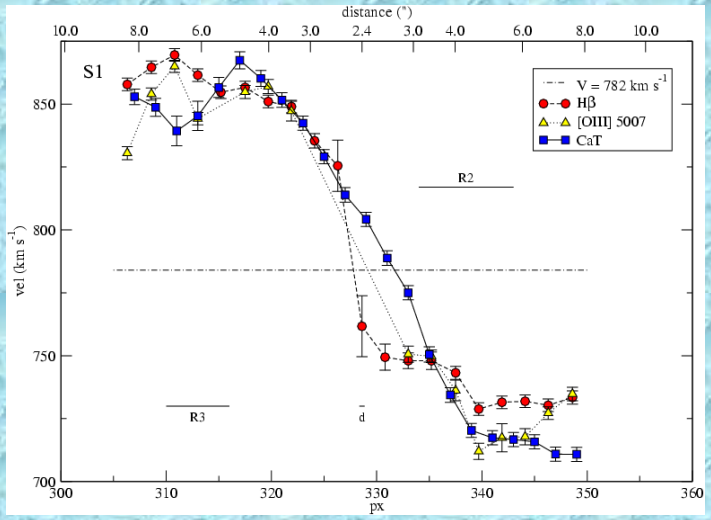


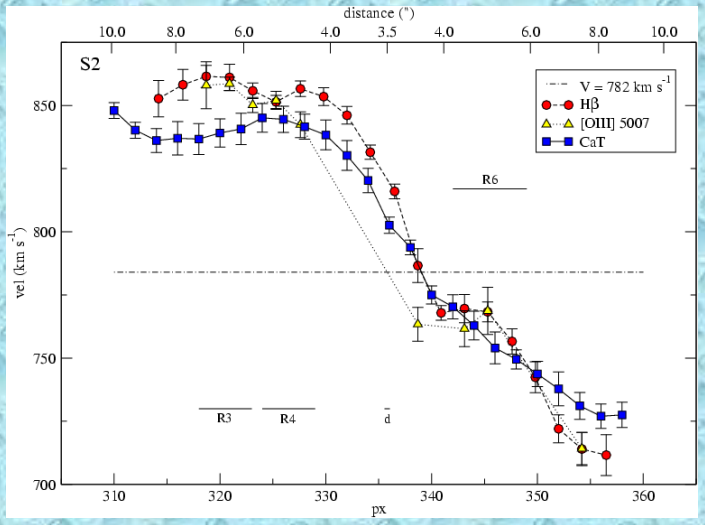


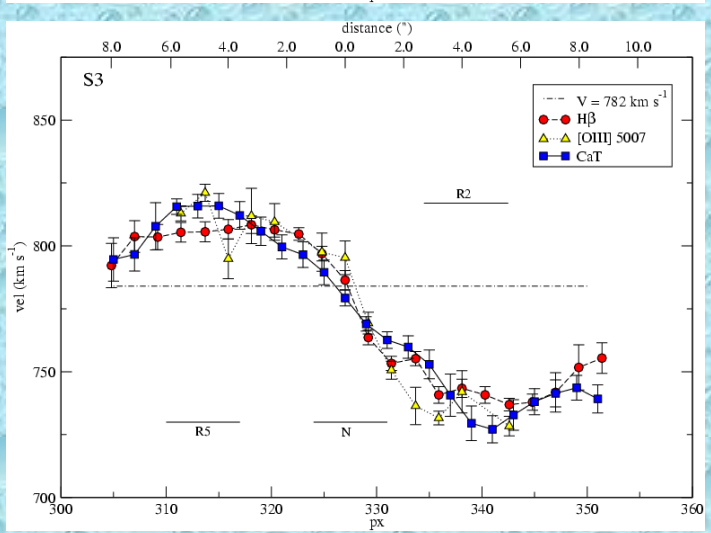
The rotation curve corresponding to the position going through the centre of the galaxy shows maximum and minimum values at the position of the circumnuclear ring, as observed in other galaxies with CNSFRs.

Summary & Conclusions

The rotation velocities derived for both stars and gas are in reasonable agreement, although in some cases the gas shows a velocity slightly different from that of the stars.







The differences in velocity between gas and stars can be interpreted as motions of the ionised hydrogen deviating from rotation and consistent with a radial infall to the central regions of the galaxy. Our results are consistent with those found by Rubin et al. (1975) **and would yield an infall velocity of about 25 km/s**.

Acknowledgments

We are indebted to Jesús López who provided the data on the SDSS sample prior to publication.

We acknowledge fruitful discussions with Horacio Dottori, Enrique Pérez, Enrique Pérez-Montero and José Vílchez.